

# First principles study of the vibronic coupling in positively charged $C_{60}^+$

Zhishuo Huang<sup>1, a)</sup> and Dan Liu<sup>2, 1, b)</sup>

<sup>1)</sup> *Theory of Nanomaterials Group, KU Leuven, Celestijnenlaan 200F, B-3001 Leuven, Belgium*

<sup>2)</sup> *Shaanxi Institute of Flexible Electronics, Northwestern Polytechnical University, 127 West Youyi Road, Xi'an, 710072, Shaanxi, China*

(Dated: 12 August 2019)

The orbital vibronic coupling parameters for  $C_{60}^+$  were derived by using frozen-phonon approach with density functional theory calculations at hybrid B3LYP functional level. Based on the derived vibronic coupling parameters, the static Jahn-Teller effect of  $C_{60}^+$  were analyzed. At the global minima of the adiabatic potential energy surface, the Jahn-Teller deformation shows a  $D_{5d}$  structure with the stabilization energy of 110 meV which is two times as large as that of  $C_{60}^-$ , suggesting the crucial role of the dynamical Jahn-Teller effect in  $C_{60}^+$ . The present coupling parameters enables us to assess the actual situation of the dynamical Jahn-Teller effect of  $C_{60}^+$  and also that of excited  $C_{60}$  in combination with the established coupling parameters for  $C_{60}^-$ .

## I. INTRODUCTION

Recent experimental confirmation of the presence of  $C_{60}^+$  in interstellar materials<sup>1,2</sup> renewed the interests in  $C_{60}$  cations, and burst various spectroscopic and theoretical investigations on  $C_{60}^+$  and related systems<sup>3-8</sup>. It is known that  $C_{60}$  in its charged and excited states exhibits complex Jahn-Teller (JT) effect due to its high point group symmetry ( $I_h$ )<sup>9,10</sup>. In particular, the JT effect of  $C_{60}^+$  is one of the most involved cases because of the five-fold degenerate highest occupied molecular orbitals (HOMOs) of  $C_{60}$ . Toward the understanding of the JT effect of  $C_{60}^+$  cations, spectroscopic<sup>11-13</sup> and theoretical<sup>14-22</sup> investigations have been piled up.

For the realistic description of JT effect of positively charged  $C_{60}$ , it is decisive to combine the adequate model and the accurate vibronic coupling parameters of  $C_{60}$  cation characterizing its JT effect. The derivation of the vibronic coupling parameters have been addressed<sup>23-25</sup>, and comprehensive sets of parameters have been estimated by density functional theory (DFT) calculations at local density approximation (LDA) level<sup>23,25</sup>. Nevertheless, in the study of  $C_{60}^-$ , it has been shown that the LDA tends to underestimate the coupling parameters<sup>26</sup>, while the hybrid B3LYP functional is found to give closer parameters to the experimental data. Furthermore, a good agreement between the B3LYP and GW approximation calculations<sup>27</sup> supports the accuracy of the hybrid functional in the study of  $C_{60}$ . Therefore, it is desired to

derive the coupling parameters at better level than LDA for accurate description of  $C_{60}$  cations.

In this work, we derived the orbital vibronic coupling parameters for  $C_{60}^+$  cations from the DFT data with B3LYP hybrid functional. The obtained vibronic coupling parameters were compared with the previous data obtained by LDA calculations. Based on these parameters, the adiabatic potential energy surface was analyzed, and the symmetry of the JT deformed  $C_{60}^+$  as well as the static JT energy was established.

## II. VIBRONIC HAMILTONIAN

The highest occupied molecular orbitals (HOMOs) of  $C_{60}$  with  $I_h$  symmetry<sup>28</sup> are characterized by five-fold degenerate  $h_u$  irreducible representation. According to the selection rule, these orbitals linearly couple to the mass-weighted normal vibrational modes involved in the symmetric product of the  $h_u$  representation<sup>29</sup>:

$$[h_u \otimes h_u] = a_g \oplus g_g \oplus 2h_g. \quad (1)$$

Among them, the  $g_g$  and  $h_g$  modes are JT active, while the  $a_g$  is not because the  $a_g$  modes do not change the symmetry of the molecule. Thus, taking the equilibrium structure of neutral  $C_{60}$  as the reference, the  $H \otimes (a \oplus g \oplus 2h)$  JT Hamiltonian for  $C_{60}^+$  is expressed as<sup>9,10,14</sup>

$$H = H_0 + H_{JT}, \quad (2)$$

$$H_0 = \frac{1}{2} (p_a^2 + \omega_a^2 q_a^2) + V_a q_a + \sum_{\gamma=a,x,y,z} \frac{1}{2} (p_{g\gamma}^2 + \omega_g^2 q_{g\gamma}^2) + \sum_{\gamma=\theta,\epsilon,\xi,\eta,\zeta} \frac{1}{2} (p_{h\gamma}^2 + \omega_h^2 q_{h\gamma}^2), \quad (3)$$

<sup>a)</sup>Electronic mail: zhishuohuang@gmail.com

<sup>b)</sup>Electronic mail: iamdliu@nwpu.edu.cn

$$\begin{aligned}
H_{\text{JT}} = V_g & \begin{pmatrix} \frac{1}{2}\sqrt{\frac{3}{2}}q_{ga} & 0 & -\frac{\phi}{4}\sqrt{\frac{5}{2}}q_{gx} & \frac{\phi^{-1}}{4}\sqrt{\frac{5}{2}}q_{gy} & \frac{1}{4}\sqrt{\frac{5}{2}}q_{gz} \\ 0 & \frac{1}{2}\sqrt{\frac{3}{2}}q_{ga} & \frac{\phi^{-2}}{4}\sqrt{\frac{5}{6}}q_{gx} & -\frac{\phi^2}{4}\sqrt{\frac{5}{6}}q_{gy} & \frac{5}{4\sqrt{6}}q_{gz} \\ -\frac{\phi}{4}\sqrt{\frac{5}{2}}q_{gx} & \frac{\phi^{-2}}{4}\sqrt{\frac{5}{6}}q_{gx} & -\frac{1}{\sqrt{6}}q_{ga} & \frac{1}{2}\sqrt{\frac{5}{6}}q_{gz} & \frac{1}{2}\sqrt{\frac{5}{6}}q_{gy} \\ \frac{\phi^{-1}}{4}\sqrt{\frac{5}{2}}q_{gy} & -\frac{\phi^2}{4}\sqrt{\frac{5}{6}}q_{gy} & \frac{1}{2}\sqrt{\frac{5}{6}}q_{gz} & -\frac{1}{\sqrt{6}}q_{ga} & \frac{1}{2}\sqrt{\frac{5}{6}}q_{gx} \\ \frac{1}{4}\sqrt{\frac{5}{2}}q_{gz} & \frac{5}{4\sqrt{6}}q_{gz} & \frac{1}{2}\sqrt{\frac{5}{6}}q_{gy} & \frac{1}{2}\sqrt{\frac{5}{6}}q_{gx} & -\frac{1}{\sqrt{6}}q_{ga} \end{pmatrix} \\
& + \frac{\sqrt{5}V_{1h}}{2} \begin{pmatrix} \frac{\sqrt{5}}{16}q_{h\theta} + \frac{3\sqrt{3}}{16}q_{h\epsilon} & \frac{3\sqrt{3}}{16}q_{h\theta} - \frac{\sqrt{5}}{16}q_{h\epsilon} & -\frac{\phi^{-2}}{4}q_{h\xi} & \frac{\phi^2}{4}q_{h\eta} & -\frac{\sqrt{5}}{4}q_{h\zeta} \\ \frac{3\sqrt{3}}{16}q_{h\theta} - \frac{\sqrt{5}}{16}q_{h\epsilon} & -\frac{\sqrt{3}\phi}{4}q_{h\xi} & -\frac{\phi^{-2}}{4}q_{h\theta} - \frac{\sqrt{3}\phi}{4}q_{h\epsilon} & \frac{\sqrt{3}\phi^{-1}}{4}q_{h\eta} & \frac{\sqrt{3}}{4}q_{h\zeta} \\ -\frac{\phi^{-2}}{4}q_{h\xi} & \frac{\sqrt{3}\phi^{-1}}{4}q_{h\eta} & 0 & 0 & 0 \\ \frac{\phi^2}{4}q_{h\eta} & \frac{\sqrt{3}\phi^{-1}}{4}q_{h\zeta} & 0 & \frac{\phi^2}{4}q_{h\theta} + \frac{\sqrt{3}\phi^{-1}}{4}q_{h\epsilon} & 0 \\ -\frac{\sqrt{5}}{4}q_{h\zeta} & 0 & 0 & 0 & -\frac{\sqrt{5}}{4}q_{h\theta} + \frac{\sqrt{3}}{4}q_{h\epsilon} \end{pmatrix} \\
& + \frac{\sqrt{5}V_{2h}}{2} \begin{pmatrix} \frac{9}{16}q_{h\theta} - \frac{\sqrt{15}}{16}q_{h\epsilon} & -\frac{\sqrt{15}}{16}q_{h\theta} - \frac{9}{16}q_{h\epsilon} & \frac{\phi}{4}q_{h\xi} & -\frac{\phi^{-1}}{4}q_{h\eta} & -\frac{1}{4}q_{h\zeta} \\ -\frac{\sqrt{15}}{16}q_{h\theta} - \frac{9}{16}q_{h\epsilon} & -\frac{9}{16}q_{h\theta} + \frac{\sqrt{15}}{16}q_{h\epsilon} & -\frac{\phi^{-2}}{4\sqrt{3}}q_{h\xi} & \frac{\phi^2}{4\sqrt{3}}q_{h\eta} & -\frac{1}{4}\sqrt{\frac{5}{3}}q_{h\zeta} \\ \frac{\phi}{4}q_{h\xi} & -\frac{\phi^{-2}}{4\sqrt{3}}q_{h\xi} & \frac{\phi}{4}q_{h\theta} - \frac{\phi^{-2}}{4\sqrt{3}}q_{h\epsilon} & \frac{1}{\sqrt{3}}q_{h\zeta} & \frac{1}{\sqrt{3}}q_{h\eta} \\ -\frac{\phi^{-1}}{4}q_{h\eta} & \frac{\phi^2}{4\sqrt{3}}q_{h\eta} & \frac{1}{\sqrt{3}}q_{h\zeta} & -\frac{\phi^{-1}}{4}q_{h\theta} + \frac{\phi^2}{4\sqrt{3}}q_{h\epsilon} & \frac{1}{\sqrt{3}}q_{h\xi} \\ -\frac{1}{4}q_{h\zeta} & -\frac{1}{4}\sqrt{\frac{5}{3}}q_{h\zeta} & \frac{1}{\sqrt{3}}q_{h\eta} & \frac{1}{\sqrt{3}}q_{h\xi} & -\frac{1}{4}q_{h\theta} - \frac{1}{4}\sqrt{\frac{5}{3}}q_{h\epsilon} \end{pmatrix}, \quad (4)
\end{aligned}$$

where  $\phi = (1 + \sqrt{5})/2$ ,  $\omega_\Gamma$  ( $\Gamma = a_g, g_g, h_g$ ) are the frequencies,  $q_\Gamma$  are the mass-weighted normal coordinates<sup>30</sup>, and  $V_\Gamma$  are the vibronic coupling parameters for the  $\Gamma$  mode. There are two vibronic couplings to each of the  $h_g$  mode because  $h_g$  representation appears twice in the selection rule, Eq. (1). The basis of the vibronic Hamiltonian matrices are the  $H_u$  electronic states of  $C_{60}^+$  in the order of  $|H_u\theta\rangle$ ,  $|H_u\epsilon\rangle$ ,  $|H_u\xi\rangle$ ,  $|H_u\eta\rangle$ ,  $|H_u\zeta\rangle$ . For the  $h_g$  and  $h_u$  representations, the basis of  $d$  orbital type are used, and hence,  $\theta, \epsilon, \xi, \eta, \zeta$  transform as  $(2z^2 - x^2 - y^2)/\sqrt{6}$ ,  $(x^2 - y^2)/\sqrt{2}$ ,  $\sqrt{2}yz$ ,  $\sqrt{2}zx$ ,  $\sqrt{2}xy$ , respectively, under rotation. Although  $C_{60}$  has two  $a_g$ , six and eight sets of  $g_g$  and  $h_g$  modes, respectively, the indices distinguishing them are not explicitly written in Eq. (3) for simplicity. The phase factor of the mass-weighted normal modes are the same as those in the Supplemental Materials of Ref. 31. For the derivation of the vibronic Hamiltonian, the Clebsch-Gordan coefficients are taken from Ref. 31, and coefficient  $\sqrt{5}/2$  is multiplied with the vibronic couplings terms to the  $h_g$  mode so that the JT stabilization energy becomes:

$$E_g^{\text{JT}} = -\frac{V_g^2}{2\omega_g^2}, \quad E_{nh}^{\text{JT}} = -\frac{V_{nh}^2}{2\omega_h^2}, \quad (n = 1, 2). \quad (5)$$

Since as the reference structure of  $C_{60}^+$ , the equilibrium geometry of  $C_{60}$  is chosen, the vibronic coupling for the totally symmetric mode is also nonzero. The stabilization by the totally symmetric deformation is

$$E_a = -\frac{V_a^2}{2\omega_a^2}. \quad (6)$$

Present basis of the irreducible representation slightly differs from that in Ref. 14. In the literature,  $\theta, \epsilon$

are the linear combination of the real  $d$ -type functions  $d_{z^2}, d_{x^2-y^2}$ :

$$q_\theta = \sqrt{\frac{3}{8}}Q_\theta + \sqrt{\frac{5}{8}}Q_\epsilon, \quad q_\epsilon = \sqrt{\frac{3}{8}}Q_\theta - \sqrt{\frac{5}{8}}Q_\epsilon, \quad (7)$$

where  $Q_\theta$  and  $Q_\epsilon$  are the coordinates in Ref. 14, while  $q_\theta$  and  $q_\epsilon$  are the coordinate in this work. The relation between the coupling parameters  $V_{1h}$  and  $V_{2h}$  in this work and  $F_{Hb}$  and  $F_{Ha}$  defined in Ref. 14 also slightly differ:

$$V_{1h} = \frac{F_{Hb}}{4\sqrt{5}}, \quad V_{2h} = \frac{F_{Ha}}{12\sqrt{5}}. \quad (8)$$

The modification introduced here is to treat the JT Hamiltonian in the framework which is consistent to the standard one of  $C_{60}^-$ <sup>9</sup>.

### III. RESULTS

#### A. Orbital vibronic coupling parameters

The vibronic coupling constants of  $C_{60}$  have been most intensively investigated in the case of  $C_{60}^-$  anion, and the coupling constants have been derived by various methods. By definition, the vibronic coupling parameters for the JT active  $h_g$  modes,  $V_{h_g}^-$ , can be derived by<sup>26</sup>

$$V_{h_g}^- = -\left. \frac{\partial E_z^-(\mathbf{q}_{h_g})}{\partial q_{h_g\theta}} \right|_{\mathbf{q}_{h_g}=\mathbf{0}}, \quad (9)$$

where  $E_z^-(\mathbf{q}_{h_g}) = \langle T_{1uz} | \hat{H}^- | T_{1uz} \rangle$ ,  $|T_{1uz}\rangle$  is the  $t_{1u}z$  electronic state of  $C_{60}^-$ ,  $\hat{H}^-$  is the Hamiltonian for  $C_{60}^-$ ,

and  $\mathbf{q}_{h_g} = \mathbf{0}$  indicates the equilibrium structure of  $C_{60}$ . Because of the symmetry, the contributions from the occupied orbitals are zero, and only the partially filled  $t_{1u}$  orbital level contribute to the vibronic coupling. In the case of  $C_{60}^-$ , the nature of the  $t_{1u}$  orbitals do not differ from that of neutral  $C_{60}$ : although the  $t_{1u}$  orbitals are modified by the mixing with the other  $t_{1u}$  orbitals, while there are not so many  $t_{1u}$  orbitals due to high symmetry and the orbitals are separated each other by large orbital energy gaps. Consequently, the gradient of the total energy can be approximated by the gradient of the orbital energy level with respect to the normal modes of neutral  $C_{60}$ . Indeed, in the case of  $C_{60}^-$ , these two approaches give very close results<sup>26,27,31,32</sup>.

Similar situation is expected in  $C_{60}^+$ : The nature of the  $h_u$  orbitals do not change by adding one hole with the same molecular structure. Thus, the orbital vibronic coupling parameters of neutral  $C_{60}$  can be used to express the vibronic coupling parameters of  $C_{60}^+$ . Since  $C_{60}^+$  has one hole in the  $h_u$  HOMOs, it is convenient to perform particle-hole transformation<sup>33</sup>. Under this transformation, the sign of the orbital vibronic coupling parameter for the HOMO level of  $C_{60}$  should be inverted in terms of the hole. Therefore,

$$V_{\Gamma} = -v_{\Gamma}, \quad (10)$$

where  $v_{\Gamma}$  is the orbital vibronic coupling parameter and  $V_{\Gamma}$  is the parameter for  $C_{60}^+$ .

The orbital vibronic coupling parameters were calculated using frozen-phonon approach. The orbital energy levels of distorted  $C_{60}$  are fitted to the eigenvalues of the JT Hamiltonian matrix (Eq. (4)). In the present case, the  $h_g(\mu)\epsilon$  and  $g_g(\mu)a$  deformations are used because the diagonalization of the model Hamiltonian is easy in this case. The DFT orbital energy levels using hybrid B3LYP exchange correlation functional and a triple-zeta basis set were taken from Ref. 31. Some of the results are shown in Fig. 15 (see for the other results Supplemental Materials). The black points indicate the DFT levels originating from HOMO, and the gray lines are the levels from the model. The derived orbital vibronic coupling parameters are shown in Table I. One should note that there is almost no nonlinear splitting due to vibronic effect in the HOMO level, indicating the weak quadratic or higher vibronic couplings as in the case of  $C_{60}^-$ <sup>31</sup>. This guarantees the validity of the use of linear vibronic model (Eq. (3)) for the description of the JT effect of  $C_{60}$  cations.

## B. Static Jahn-Teller effect

The vibronic coupling lifts the degeneracy with the deformation keeping one of the highest subgroup symmetries<sup>34</sup>, resulting in six  $D_{5d}$  and ten  $D_{3d}$  minima<sup>14</sup>, because there are six  $C_5$  and ten  $C_3$  axes in  $C_{60}$ . Thus, based on the present basis of the representation, using the symmetry adapted deformations<sup>20</sup>, the deformation

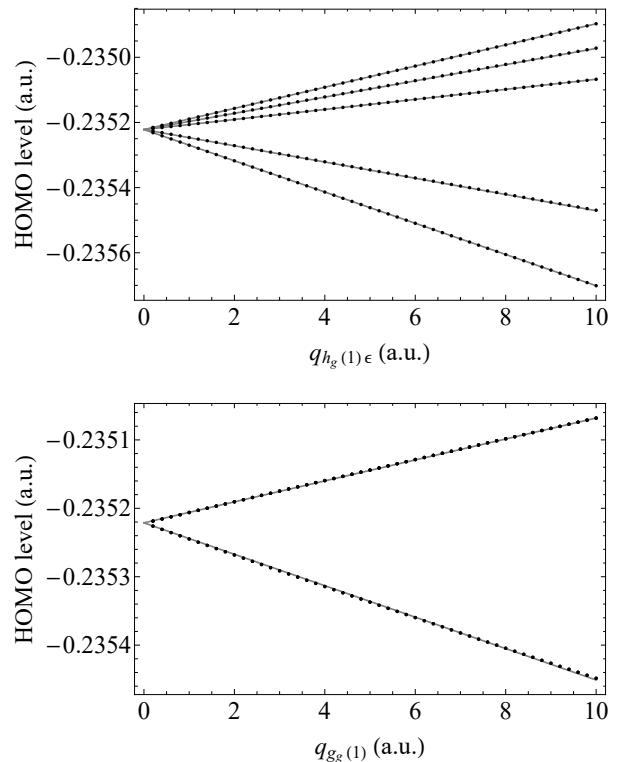


FIG. 1. The JT splitting of the HOMO levels with respect to  $q_{h_g(1)\epsilon}$  (top) and  $q_{g_g(1)a}$  (down) deformations (in atomic unit). The black points and gray lines indicate the DFT values and model energy, respectively.

for  $D_{5d}$  and  $D_{3d}$  minima are expressed by

$$\begin{aligned} \mathbf{q}_{h_g}^{D_{5d}} &= q_{h_g} \left( \frac{\phi^2}{2\sqrt{5}}, \frac{\phi^{-1}}{2} \sqrt{\frac{3}{5}}, 0, \sqrt{\frac{3}{5}}, 0 \right), \\ \mathbf{q}_{g_g}^{D_{5d}} &= q_{g_g} (0, 0, 0, 0), \end{aligned} \quad (11)$$

and

$$\begin{aligned} \mathbf{q}_{h_g}^{D_{3d}} &= q_{h_g} \left( -\frac{\phi^{-1}}{2}, \frac{\phi^2}{2\sqrt{3}}, 0, \frac{1}{\sqrt{3}}, 0 \right), \\ \mathbf{q}_{g_g}^{D_{3d}} &= q_{g_g} \left( \frac{1}{\sqrt{6}}, 0, -\sqrt{\frac{5}{6}}, 0 \right), \end{aligned} \quad (12)$$

respectively<sup>31</sup>. Substituting these symmetrized deformations, Eqs. (11) and (12), into the potential terms in the model Hamiltonian (kinetic energy term is ignored), and then diagonalizing the Hamiltonian, we obtain the lowest adiabatic potential energies as

$$\begin{aligned} U^{D_{5d}} &= \frac{1}{2}\omega_h^2 q_h^2 + V_{1h} q_h, \\ U^{D_{3d}} &= \frac{1}{2}\omega_g^2 q_g^2 + \frac{1}{2}\omega_h^2 q_h^2 + \frac{1}{3} \left( 2V_g q_g + \sqrt{5}V_{2h} q_h \right) \end{aligned} \quad (13)$$

for  $D_{5d}$  and  $D_{3d}$  deformations, respectively. The energies of the global minima are expressed in terms of the



data are shown in Table II. These data shows that the JT energies obtained by B3LYP are larger than those from LDA or PBE-related methods. In particular, compared with the present data with that by Manini *et al.*,<sup>23</sup> the latter is only about 60 % of the present data. The underestimation of the JT energy by LDA method is consistent with the case of  $C_{60}^-$ .<sup>26</sup> The B3LYP data from Ref. 7 and the present one are close to each other, whereas the former is larger than the latter by 11 meV. Such a difference is expected to come from that the stabilization energy due to the totally symmetric modes, Eq. (6), is included in Ref. 7. The stabilization obtained in the present calculation is about 3.5 meV (Table I), which is smaller than 11 meV. The underestimate of the vibronic coupling to the totally symmetric mode comes from the lack of the contributions from the occupied orbitals. In general, only the partially filled frontier orbitals contribute to the vibronic coupling to the JT modes due to the symmetry<sup>42</sup>, whereas all the occupied orbitals do contribute to the vibronic coupling to the totally symmetric modes<sup>43</sup>. Another possible origin of the discrepancy is nonlinear vibronic coupling, however, the effect is much weaker than that by linear vibronic coupling as in  $C_{60}$  anions<sup>31</sup>.

TABLE II. Jahn-Teller energies of  $C_{60}^+$  (meV).

Functional	Method	$D_{5d}$	$D_{3d}$	Ref
B3LYP	(I)	110	30	Present
LDA	(I)	69	22	23
B3LYP	(II)	121	-	7
LDA	(III)	74	27	25
OPBE	(III)	74	28	25
B3LYP	(III)	80	32	25
PBE	(III)	74	28	41
LDA	(IV)	72	20	25
OPBE	(IV)	74	21	25
B3LYP	(IV)	94	25	25

On the other hand, the B3LYP data obtained by methods (III) and (IV)<sup>25</sup> tend to be smaller than the other B3LYP data (present and Ref. 7). Since these methods with LDA give similar data as the one by method (I),<sup>23</sup> the methods themselves would not be the origin of the discrepancy seen in B3LYP data. Thus, a possible reason is that the deformed geometry with B3LYP functional in Ref. 25 is the one at a local minima.

Besides these works, we note that Kern *et al.*<sup>13</sup> have optimized the structure to simulate infrared (IR) absorption spectrum with BP86 functional, while JT energy was not derived.

#### IV. DISCUSSION

In order to fully reveal the molecular nature of  $C_{60}^+$ , the nonadiabatic dynamical Jahn-Teller effect is crucial. The

most straightforward way would be the exact diagonalization of the molecular Hamiltonian fully quantizing the nuclear as well as electronic coordinates, nevertheless, it is not practical. To partly overcome this difficulty, the use of model Jahn-Teller Hamiltonian (3) with accurate vibronic coupling parameters are indispensable to derive low-energy states.

The vibronic coupling parameters of  $C_{60}^+$  have been derived by using DFT calculations with LDA<sup>23,25</sup> and B3LYP<sup>24</sup> functionals. As discussed in Sec. II, the model Hamiltonian is described by one vibronic coupling parameter for each of the  $a_g$  and  $g_g$  mode, and two parameters for each of the  $h_g$  mode. Both parameters for the  $h_g$  modes,  $V_{1h}$  and  $V_{2h}$ , have been derived only in Ref. 23 and Ref. 25, while they have not in Ref. 24. Ramanantoina *et al.*<sup>25</sup> shows that the magnitudes of the derived coupling parameters obtained from the gradient of HOMO level<sup>23</sup> and those from adiabatic potential energy surface agree well with each other, which has been also seen in  $C_{60}^-$ .<sup>26,31,32</sup> Thus, the present orbital vibronic coupling parameters derived from  $C_{60}$  must be close to the parameters for  $C_{60}^+$  derived based on the definition.

The accuracy of the LDA data have been discussed<sup>25,44</sup> based on the comparison between the experimental photoelectron spectra (PES)<sup>12</sup> and those from numerical simulation<sup>17</sup>. Indeed, the PES is very useful to establish the vibronic coupling parameters, whereas the simulation of the PES requires high accuracy both in theoretical simulation and experiments. In the case of  $C_{60}^-$ , the vibronic coupling parameters derived from the broad PES at high-temperature<sup>45</sup> have been proved to be overestimated by the simulation of the high-resolution PES spectra<sup>26</sup>. Furthermore, it was also found that the error bar of the vibronic coupling parameters derived from the broad PES is very large<sup>26</sup>. Thus, the derivation of the accurate coupling parameters is only possible if we have high-resolution PES spectra measured at low-temperature<sup>46,47</sup>. In the case of  $C_{60}^+$ , as pointed out by Manini *et al.*<sup>17</sup>, the experimental PES is broad and the fine structure of low-energy region due to vibronic coupling is completely smeared out, which prevents the direct comparison between the theory and experiment. Moreover, in the case of PES of  $C_{60}^+$ , the theoretical ratio of the second strongest peak to the strongest one is smaller than those of experimental data, implying the underestimation of the vibronic coupling by LDA. From this point, the present B3LYP data larger than the LDA data by 40 % would give better agreement.

The quality of the B3LYP calculations has been checked in  $C_{60}$  anions by comparing the theory and experimental data. Besides the good agreement between the coupling parameters from B3LYP calculations and high-resolution PES<sup>26</sup>, the good quality of the B3LYP calculations also has been confirmed from the Néel temperature<sup>48</sup>, the spin gap<sup>49</sup>, and the explanation of the origin of the temperature evolution of infrared spectra<sup>50</sup> of Mott-insulating  $Cs_3C_{60}$  using the same vibronic coupling parameters. Furthermore, the vibronic



coupling parameters from the B3LYP calculations tend to give good description of the inelastic electron tunneling spectra of other organic molecule<sup>51</sup>. Thus, it must be natural to expect that the B3LYP values are closer to the reality in  $C_{60}^+$ .

In the case of  $C_{60}^+$ , accurate calculations of vibronic states are difficult using the program used for  $C_{60}^-$  in Refs. 31 and 49 because larger vibronic basis is required due to the stronger vibronic coupling, highly degenerate electronic states, the larger number of the JT active modes, and the lack of Lie group symmetry. Ponzellini has checked the convergence of the ground vibronic states of  $C_{60}^-$  and concluded that with the Gunnarsson *et al*'s data the convergence is achieved with vibrational excitation of 6<sup>44</sup>, though it seems to be too small according to our criterion. Ponzellini also has demonstrated the convergence of the ground vibronic states of  $C_{60}^+$  with a smartly chosen of the vibronic basis.<sup>44</sup> In the study, the vibronic basis has to include up to 10 harmonic vibrational excitation for the lowest frequency modes. Since the test calculations were done using the data of Manini *et al.*<sup>23</sup>, to perform the calculations with the present data much larger basis is required. In order to simulate experimental data, improvement of the program is decisive, and hence, we postpone the study of vibronic states of  $C_{60}^+$ .

Although the derivation of the vibronic coupling parameters is the first step toward the description of the molecular states of  $C_{60}^+$ , we believe this is a crucial step. Once the simulation of accurate vibronic states become possible, it is possible to interpret various spectra such as scanning tunneling measurements of  $C_{60}$ <sup>52</sup>, inverse PES<sup>53</sup> and angle resolved PES<sup>54</sup> to mention a few. Furthermore, the present coupling parameters are derived based on the well-defined phase factor of the normal mode which has been also used for the orbital coupling parameters for LUMO<sup>31</sup> and next LUMO<sup>55</sup>. Therefore, by combining the present coupling parameters with them, it is also possible to address the complex vibronic problems of excited  $C_{60}$ <sup>56</sup>, and also to analyze *e.g.* luminescence spectra<sup>57</sup> and relaxation process and thermally activated delayed luminescence<sup>58</sup>.

## V. CONCLUSIONS

In this work, the orbital vibronic coupling parameters for the  $h_u$  HOMO level of  $C_{60}$  are derived using B3LYP hybrid functional. With the obtained coupling parameters, the JT stabilization energies of  $C_{60}^+$  are calculated, and the JT structure at the minima of the adiabatic potential energy surface is confirmed to be  $D_{5d}$ . The JT stabilization energy of  $C_{60}^+$  is about two times larger than  $C_{60}^-$ , suggesting the crucial role of the dynamical JT effect to reveal the actual situation of  $C_{60}^+$ .

The present coupling parameters have been derived within the same framework used for our studies on the ground and the excited  $C_{60}^-$ . Thus, combining the data of the present and the other works, it is also possible to

analyze the vibronic problems of excited  $C_{60}$ .

## ACKNOWLEDGMENTS

The authors thank Naoya Iwahara and Liviu Chibotaru for fruitful discussions. They also gratefully acknowledge funding by the China Scholarship Council (CSC).

- <sup>1</sup>E. K. Campbell, M. Holz, D. Gerlich, and J. P. Maier, "Laboratory confirmation of  $C_{60}^+$  as the carrier of two diffuse interstellar bands," *Nature* **523**, 322 (2015).
- <sup>2</sup>E. K. Campbell, M. Holz, J. P. Maier, D. Gerlich, G. A. H. Walker, and D. Bohlender, "Gas Phase Absorption Spectroscopy of  $C_{60}^+$  and  $C_{70}^+$  in a Cryogenic Ion Trap: Comparison with Astronomical Measurements," *The Astrophysical Journal* **822**, 17 (2016).
- <sup>3</sup>S. Spieler, M. Kuhn, J. Postler, M. Simpson, R. Wester, P. Scheier, W. Ubachs, X. Bacalla, J. Bouwman, and H. Linnartz, " $C_{60}^+$  and the Diffuse Interstellar Bands: An Independent Laboratory Check," *The Astrophysical Journal* **846**, 168 (2017).
- <sup>4</sup>K. M. Yamada, S. C. Ross, and F. Ito, "<sup>13</sup>C-substituted  $C_{60}^+$ : Predictions of the rotational spectra," *Molecular Astrophysics* **6**, 9 – 15 (2017).
- <sup>5</sup>D. V. Strelnikov, J. Jašík, D. Gerlich, M. Murata, Y. Murata, K. Komatsu, and J. Roithová, "Near- and Mid-IR Gas-Phase Absorption Spectra of  $H_2@C_{60}^+-He$ ," *The Journal of Physical Chemistry A* **122**, 8162–8166 (2018).
- <sup>6</sup>A. Kaiser, J. Postler, M. Onćák, M. Kuhn, M. Renzler, S. Spieler, M. Simpson, M. Gatchell, M. K. Beyer, R. Wester, F. A. Gianturco, P. Scheier, F. Calvo, and E. Yurtsever, "Isomeric Broadening of  $C_{60}^+$  Electronic Excitation in Helium Droplets: Experiments Meet Theory," *The Journal of Physical Chemistry Letters* **9**, 1237–1242 (2018).
- <sup>7</sup>A. O. Lykhin, S. Ahmadvand, and S. A. Varganov, "Electronic Transitions Responsible for  $C_{60}^+$  Diffuse Interstellar Bands," *The Journal of Physical Chemistry Letters* **10**, 115–120 (2019).
- <sup>8</sup>M. A. Cordiner, H. Linnartz, N. L. J. Cox, J. Cami, F. Najjarro, C. R. Proffitt, R. Lallement, P. Ehrenfreund, B. H. Foring, T. R. Gull, P. J. Sarre, and S. B. Charnley, "Confirming interstellar  $c_{60}^+$  using the hubble space telescope," *The Astrophysical Journal* **875**, L28 (2019).
- <sup>9</sup>C. C. Chancey and M. C. M. O'Brien, *The Jahn-Teller Effect in  $C_{60}$  and Other Icosahedral Complexes* (Princeton University Press, Princeton, 1997).
- <sup>10</sup>I. B. Bersuker, *The Jahn-Teller Effect* (Cambridge University Press, Cambridge, 2006).
- <sup>11</sup>P. A. Brühwiler, A. J. Maxwell, P. Baltzer, S. Andersson, D. Arvanitis, L. Karlsson, and N. Mårtensson, "Vibronic coupling in the photoemission bands of condensed  $C_{60}$ ," *Chemical Physics Letters* **279**, 85 – 91 (1997).
- <sup>12</sup>S. E. Canton, A. J. Yencha, E. Kukuk, J. D. Bozek, M. C. A. Lopes, G. Snell, and N. Berrah, "Experimental Evidence of a Dynamic Jahn-Teller Effect in  $C_{60}^+$ ," *Phys. Rev. Lett.* **89**, 045502 (2002).
- <sup>13</sup>B. Kern, D. Strelnikov, P. Weis, A. Böttcher, and M. M. Kappes, "IR Absorptions of  $C_{60}^+$  and  $C_{60}^-$  in Neon Matrixes," *J. Phys. Chem. A* **117**, 8251 (2013).
- <sup>14</sup>A. Ceulemans and P. W. Fowler, "The Jahn-Teller instability of fivefold degenerate states in icosahedral molecules," *The Journal of Chemical Physics* **93**, 1221–1234 (1990).
- <sup>15</sup>C. P. Moate, M. C. M. O'Brien, J. L. Dunn, C. A. Bates, Y. M. Liu, and V. Z. Polinger, " $H \otimes h$ : A Jahn-Teller Coupling That Really Does Reduce the Degeneracy of the Ground State," *Phys. Rev. Lett.* **77**, 4362–4365 (1996).
- <sup>16</sup>P. De Los Rios, N. Manini, and E. Tosatti, "Dynamical Jahn-Teller effect and Berry phase in positively charged fullerenes: Basic considerations," *Phys. Rev. B* **54**, 7157–7167 (1996).

- <sup>17</sup>N. Manini, P. Gattari, and E. Tosatti, "Jahn-Teller Spectral Fingerprint in Molecular Photoemission:  $C_{60}$ ," *Phys. Rev. Lett.* **91**, 196402 (2003).
- <sup>18</sup>E. Lijnen and A. Ceulemans, "Berry phase and entanglement in the icosahedral  $H \otimes (g \oplus 2h)$  Jahn-Teller system with trigonal minima," *Phys. Rev. B* **71**, 014305 (2005).
- <sup>19</sup>I. D. Hands, L. M. Sindi, J. L. Dunn, and C. A. Bates, "Theoretical treatment of pseudorotation in the Jahn-Teller  $C_{60}^+$  ion," *Phys. Rev. B* **74**, 115410 (2006).
- <sup>20</sup>I. D. Hands, J. L. Dunn, W. A. Diery, and C. A. Bates, "Vibronic coupling in the icosahedral  $C_{60}^{2+}$  Jahn-Teller cation: Repercussions of the nonsimple reducibility of the  $H \otimes H$  product," *Phys. Rev. B* **73**, 115435 (2006).
- <sup>21</sup>I. D. Hands, W. A. Diery, C. A. Bates, and J. L. Dunn, "Jahn-teller effects in the  $C_{60}^{2+}$  cation undergoing  $D_{2h}$  distortion," *Phys. Rev. B* **76**, 085426 (2007).
- <sup>22</sup>A. Ceulemans, E. Lijnen, P. W. Fowler, R. B. Mallion, and T. Pisanski, "S5 graphs as model systems for icosahedral jahn-teller problems," *Theoretical Chemistry Accounts* **131** (2012), 10.1007/s00214-012-1246-5.
- <sup>23</sup>N. Manini, A. D. Corso, M. Fabrizio, and E. Tosatti, "Electron-vibration coupling constants in positively charged fullerene," *Philosophical Magazine B* **81**, 793–812 (2001).
- <sup>24</sup>M. Saito, "Electron-phonon coupling of electron- or hole-injected  $C_{60}$ ," *Phys. Rev. B* **65**, 220508 (2002).
- <sup>25</sup>H. Ramanantoanina, M. Zlatar, P. García-Fernández, C. Daul, and M. Gruden-Pavlović, "General treatment of the multimode jahn-teller effect: study of fullerene cations," *Phys. Chem. Chem. Phys.* **15**, 1252–1259 (2013).
- <sup>26</sup>N. Iwahara, T. Sato, K. Tanaka, and L. F. Chibotaru, "Vibronic coupling in  $C_{60}^-$  anion revisited: Derivations from photoelectron spectra and DFT calculations," *Phys. Rev. B* **82**, 245409 (2010).
- <sup>27</sup>C. Faber, J. L. Janssen, M. Côté, E. Runge, and X. Blase, "Electron-phonon coupling in the  $C_{60}$  fullerene within the many-body *GW* approach," *Phys. Rev. B* **84**, 155104 (2011).
- <sup>28</sup>H. W. Kroto, J. R. Heath, S. C. O'Brien, R. F. Curl, and R. E. Smalley, " $C_{60}$ : Buckminsterfullerene," *Nature* **318**, 162–163 (1985).
- <sup>29</sup>H. A. Jahn and E. Teller, "Stability of Polyatomic Molecules in Degenerate Electronic States. I. Orbital Degeneracy," *Proc. R. Soc. Lond. A* **161**, 220 (1937).
- <sup>30</sup>T. Inui, Y. Tanabe, and Y. Onodera, *Group Theory and Its Applications in Physics* (Springer-Verlag, Berlin and Heidelberg, 1990).
- <sup>31</sup>D. Liu, Y. Niwa, N. Iwahara, T. Sato, and L. F. Chibotaru, "Quadratic Jahn-Teller effect of fullerene anions," *Phys. Rev. B* **98**, 035402 (2018).
- <sup>32</sup>J. Laflamme Janssen, M. Côté, S. G. Louie, and M. L. Cohen, "Electron-phonon coupling in  $C_{60}$  using hybrid functionals," *Phys. Rev. B* **81**, 073106 (2010).
- <sup>33</sup>A. L. Fetter and D. Walecka, *Quantum Theory of Many-Particle Systems* (Dover Publishing, Inc., New York, 2003).
- <sup>34</sup>A. D. Liehr, "Topological aspects of the conformational stability problem. Part I. Degenerate electronic states," *J. Phys. Chem.* **67**, 389 (1963).
- <sup>35</sup>V. P. Khlopin, V. Z. Polinger, and I. B. Bersuker, "The jahn-teller effect in icosahedral molecules and complexes," *Theoretica chimica acta* **48**, 87–101 (1978).
- <sup>36</sup>I. B. Bersuker and V. Z. Polinger, *Vibronic Interactions in Molecules and Crystals* (Springer-Verlag, Berlin, 1989).
- <sup>37</sup>R. Bruyndonckx, C. Daul, P. T. Manoharan, and E. Deiss, "A nonempirical approach to ground-state jahn-teller distortion: case study of  $vcl_4$ ," *Inorganic Chemistry* **36**, 4251–4256 (1997).
- <sup>38</sup>M. Zlatar, C.-W. Schlöpfer, and C. Daul, "A new method to describe the multimode jahn-teller effect using density functional theory," in *The Jahn-Teller Effect* (Springer, 2009) pp. 131–165.
- <sup>39</sup>M. Zlatar, M. Gruden-Pavlović, C.-W. Schlöpfer, and C. Daul, "Intrinsic distortion path in the analysis of the jahn-teller effect," *Journal of Molecular Structure: THEOCHEM* **954**, 86–93 (2010).
- <sup>40</sup>M. Zlatar and M. Gruden, "Calculation of the jahn-teller parameters with dft," 2019, 1 (2019).
- <sup>41</sup>J. T. Muya, H. Ramanantoanina, C. Daul, M. T. Nguyen, G. Gopakumar, and A. Ceulemans, "Jahn-Teller instability in cationic boron and carbon buckyballs  $B_{80}^+$  and  $C_{60}^+$ : a comparative study," *Phys. Chem. Chem. Phys.* **15**, 2829–2835 (2013).
- <sup>42</sup>T. Sato, K. Tokunaga, and K. Tanaka, "Vibronic coupling in cyclopentadienyl radical: A method for calculation of vibronic coupling constant and vibronic coupling density analysis," *J. Chem. Phys.* **124**, 024314 (2006).
- <sup>43</sup>T. Sato, K. Tokunaga, and K. Tanaka, "Vibronic Coupling in Naphthalene Anion: Vibronic Coupling Density Analysis for Totally Symmetric Vibrational Modes," *J. Phys. Chem. A* **112**, 758 (2008).
- <sup>44</sup>P. Ponzellini, *Computation of the paramagnetic g-factor for the fullerene monocation and monoanion*, Master's thesis, Milan University (2014).
- <sup>45</sup>O. Gunnarsson, H. Handschuh, P. S. Bechthold, B. Kessler, G. Ganteför, and W. Eberhardt, "Photoemission Spectra of  $C_{60}^-$ : Electron-Phonon Coupling, Jahn-Teller Effect, and Superconductivity in the Fullerides," *Phys. Rev. Lett.* **74**, 1875 (1995).
- <sup>46</sup>X.-B. Wang, H.-K. Woo, and L.-S. Wang, "Vibrational cooling in a cold ion trap: Vibrationally resolved photoelectron spectroscopy of cold  $C_{60}^-$  anions," *J. Chem. Phys.* **123**, 051106 (2005).
- <sup>47</sup>D. L. Huang, P. D. Dau, H. T. Liu, and L. S. Wang, "High-resolution photoelectron imaging of cold  $C_{60}^-$  anions and accurate determination of the electron affinity of  $C_{60}$ ," *J Chem Phys* **140**, 224315 (2014).
- <sup>48</sup>N. Iwahara and L. F. Chibotaru, "Dynamical Jahn-Teller Effect and Antiferromagnetism in  $Cs_3C_{60}$ ," *Phys. Rev. Lett.* **111**, 056401 (2013).
- <sup>49</sup>D. Liu, N. Iwahara, and L. F. Chibotaru, "Dynamical jahn-teller effect of fullerene anions," *Phys. Rev. B* **97**, 115412 (2018).
- <sup>50</sup>Y. Matsuda, N. Iwahara, K. Tanigaki, and L. F. Chibotaru, "Manifestation of vibronic dynamics in infrared spectra of mott insulating fullerides," *Phys. Rev. B* **98**, 165410 (2018).
- <sup>51</sup>K. Shizu, T. Sato, and K. Tanaka, "Inelastic electron tunneling spectra and vibronic coupling density analysis of 2,5-dimercapto-1,3,4-thiadiazole and tetrathiafulvalene dithiol," *Nanoscale* **2**, 2186–2194 (2010).
- <sup>52</sup>T. Frederiksen, K. J. Franke, A. Arnau, G. Schulze, J. I. Pascual, and N. Lorente, "Dynamic Jahn-Teller effect in electronic transport through single  $C_{60}$  molecules," *Phys. Rev. B* **78**, 233401 (2008).
- <sup>53</sup>C. Große, P. Merino, A. Rosławska, O. Gunnarsson, K. Kuhnke, and K. Kern, "Submolecular Electroluminescence Mapping of Organic Semiconductors," *ACS Nano* **11**, 1230–1237 (2017).
- <sup>54</sup>D. W. Latzke, C. Ojeda-Aristizabal, J. D. Denlinger, R. Reno, A. Zettl, and A. Lanzara, "Orbital character effects in the photon energy and polarization dependence of pure  $c_{60}$  photoemission," arXiv:1905.00119 (2019).
- <sup>55</sup>Z. Huang and D. Liu, "Dynamical Jahn-Teller effect in the first excited  $C_{60}^-$ ," arXiv:1905.10783 (2019).
- <sup>56</sup>Q. C. Qiu, L. F. Chibotaru, and A. Ceulemans, "Product jahn-teller systems: The  $\{T_1 \oplus H\} \otimes (g \oplus 2h)$  icosahedral exciton," *Phys. Rev. B* **65**, 035104 (2001).
- <sup>57</sup>I. Akimoto and K.-i. Kan'no, "Photoluminescence and Near-Edge Optical Absorption in the Low-Temperature Phase of Pristine  $C_{60}$  Single Crystals," *Journal of the Physical Society of Japan* **71**, 630–643 (2002).
- <sup>58</sup>A. G. Stepanov, M. T. Portella-Oberli, A. Sassara, and M. Chergui, "Ultrafast intramolecular relaxation of  $C_{60}$ ," *Chemical Physics Letters* **358**, 516 – 522 (2002).

**Supplement Material: First principles study of the vibronic coupling in positively charged  $C_{60}^+$** Zhishuo Huang<sup>1,a)</sup> and Dan Liu<sup>2,1,b)</sup><sup>1</sup>*Theory of Nanomaterials Group, KU Leuven, Celestijnenlaan 200F, B-3001 Leuven, Belgium*<sup>2</sup>*Shaanxi Institute of Flexible Electronics, Northwestern Polytechnical University, 127 West Youyi Road, Xi'an, 710072, Shaanxi, China*<sup>a)</sup>Electronic address: zhishuohuang@gmail.com<sup>b)</sup>Electronic address: iamdliu@nwpu.edu.cn

The DFT data with B3LYP hybrid functional and the definition of the phase factors of the normal modes are taken from Ref. 31. The fitting for of the DFT HOMO levels to the model hamiltonian for  $q_{h_g(i)\epsilon}$ ,  $i = 1, 2, 3, 4, 5, 6, 7, 8$  and  $q_{g_g(i)}$ ,  $i = 1, 2, 3, 4, 5, 6$  are shown.



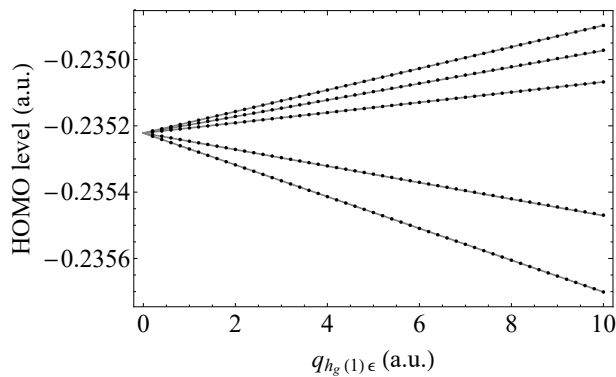


FIG. 2. The JT splitting of the HOMO levels with respect to  $q_{h_g(1)}\epsilon$  deformation (in atomic unit). The black points and gray lines indicate the DFT values and model energy, respectively.

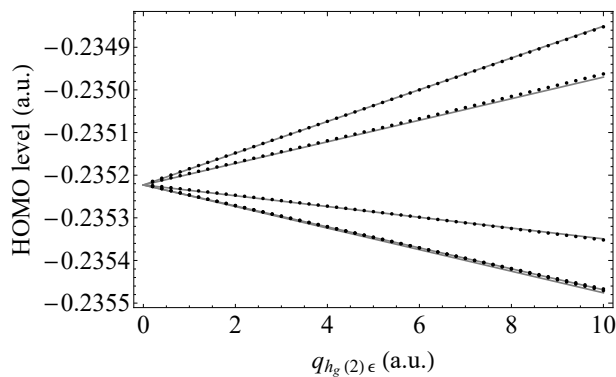


FIG. 3. The JT splitting of the HOMO levels with respect to  $q_{h_g(2)}\epsilon$  deformation (in atomic unit). The black points and gray lines indicate the DFT values and model energy, respectively.

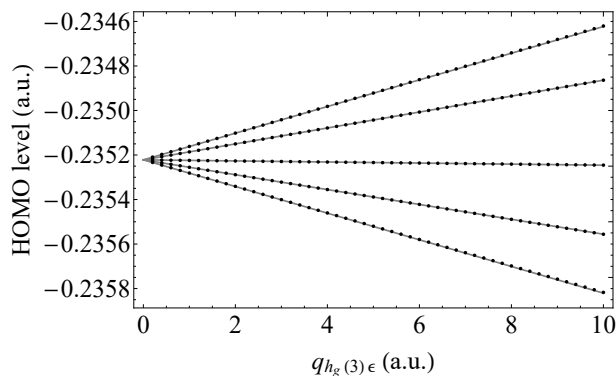


FIG. 4. The JT splitting of the HOMO levels with respect to  $q_{h_g(3)}\epsilon$  deformation (in atomic unit). The black points and gray lines indicate the DFT values and model energy, respectively.

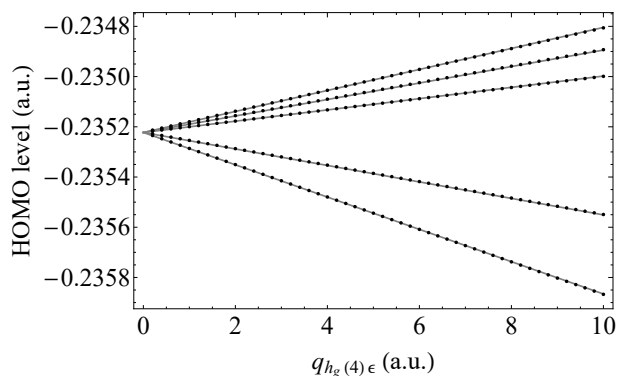


FIG. 5. The JT splitting of the HOMO levels with respect to  $q_{h_g(4)}\epsilon$  deformation (in atomic unit). The black points and gray lines indicate the DFT values and model energy, respectively.

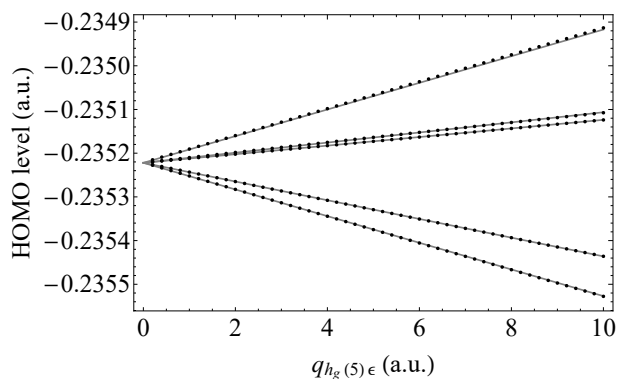


FIG. 6. The JT splitting of the HOMO levels with respect to  $q_{h_g(5)}\epsilon$  deformation (in atomic unit). The black points and gray lines indicate the DFT values and model energy, respectively.

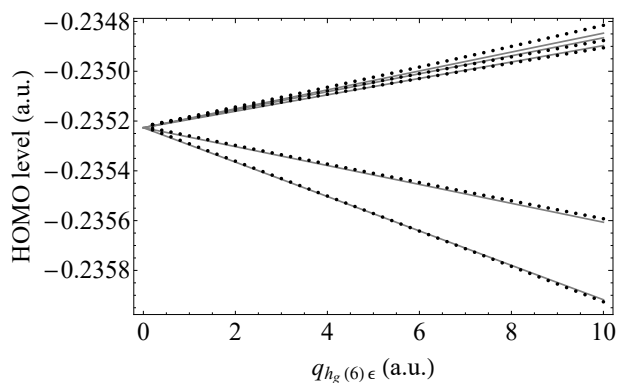


FIG. 7. The JT splitting of the HOMO levels with respect to  $q_{h_g(6)}\epsilon$  deformation (in atomic unit). The black points and gray lines indicate the DFT values and model energy, respectively.

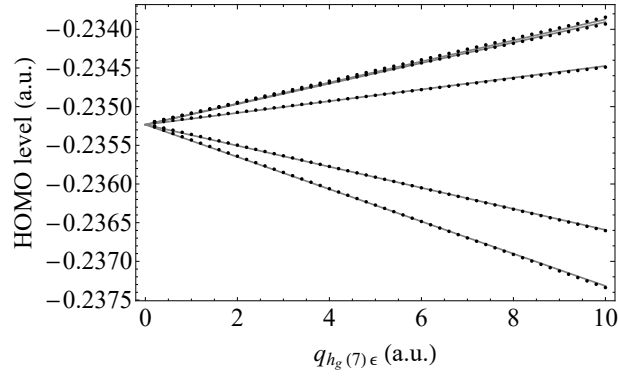


FIG. 8. The JT splitting of the HOMO levels with respect to  $q_{h_g(7)}\epsilon$  deformation (in atomic unit). The black points and gray lines indicate the DFT values and model energy, respectively.

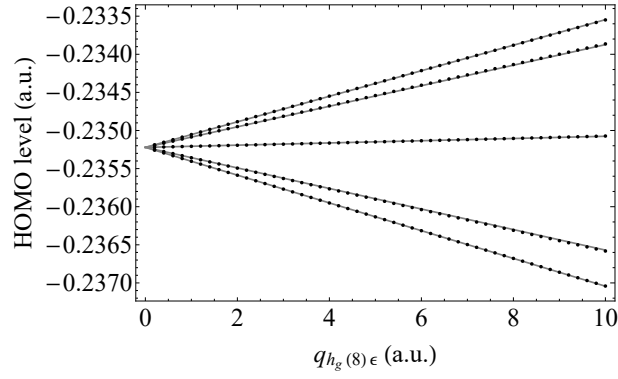


FIG. 9. The JT splitting of the HOMO levels with respect to  $q_{h_g(8)}\epsilon$  deformation (in atomic unit). The black points and gray lines indicate the DFT values and model energy, respectively.

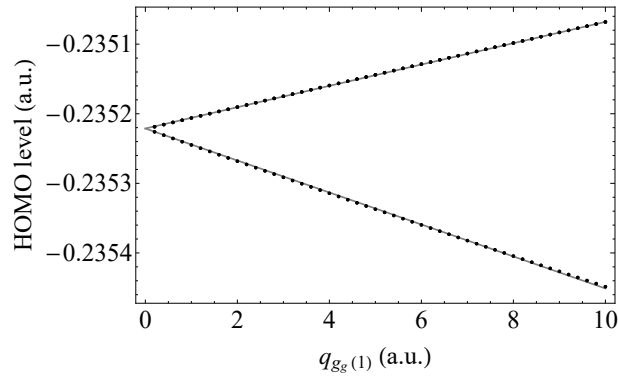


FIG. 10. The JT splitting of the HOMO levels with respect to  $q_{g_g(1)}$  deformation (in atomic unit). The black points and gray lines indicate the DFT values and model energy, respectively.

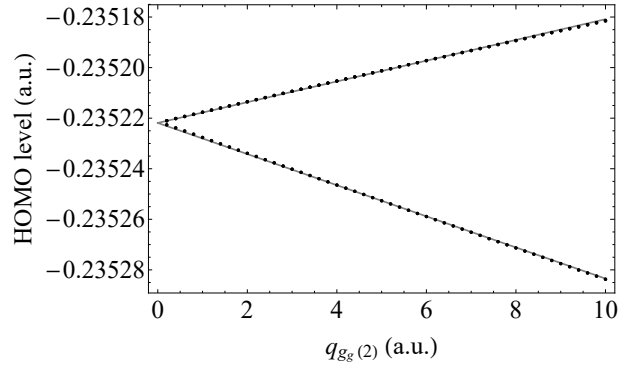


FIG. 11. The JT splitting of the HOMO levels with respect to  $q_{g_g(2)}$  deformation (in atomic unit). The black points and gray lines indicate the DFT values and model energy, respectively.

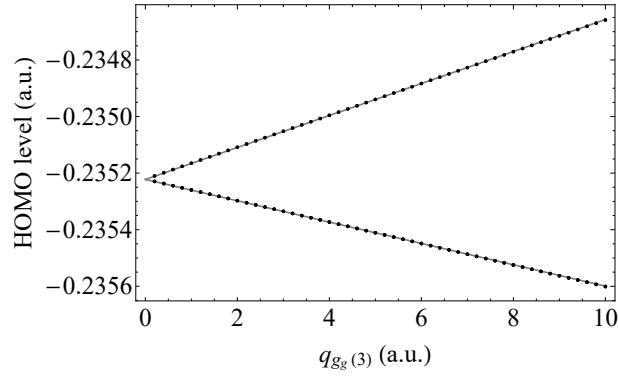


FIG. 12. The JT splitting of the HOMO levels with respect to  $q_{g_g(3)}$  deformation (in atomic unit). The black points and gray lines indicate the DFT values and model energy, respectively.

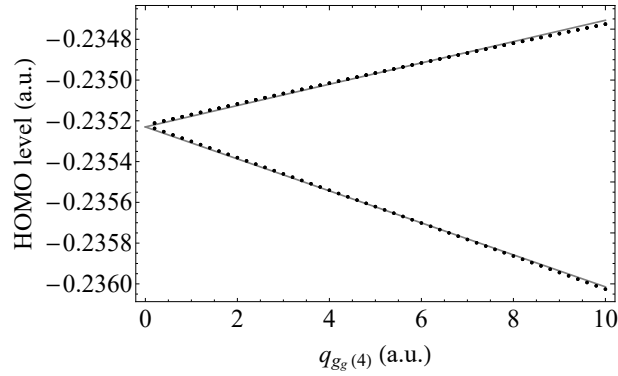


FIG. 13. The JT splitting of the HOMO levels with respect to  $q_{g_g(4)}$  deformation (in atomic unit). The black points and gray lines indicate the DFT values and model energy, respectively.

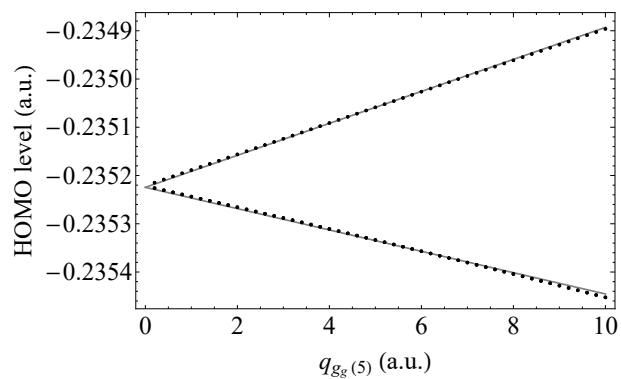


FIG. 14. The JT splitting of the HOMO levels with respect to  $q_{gg(5)}$  deformation (in atomic unit). The black points and gray lines indicate the DFT values and model energy, respectively.

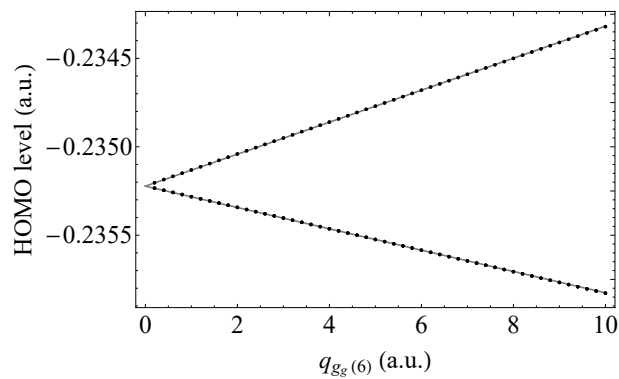


FIG. 15. The JT splitting of the HOMO levels with respect to  $q_{gg(6)}$  deformation (in atomic unit). The black points and gray lines indicate the DFT values and model energy, respectively.